MARS imaging and reconstruction challenges

Niels J. A. de Ruiter[†‡¶], Philip H. Butler[*†‡§], Anthony P. H. Butler[*†‡§],
Stephen T. Bell[‡], Alexander I. Chernoglazov[‡¶], and Michael F. Walsh[‡]
[*]Department of Physics and Astronomy, University of Canterbury, New Zealand
[†]Department of Radiology, University of Otago, New Zealand
[‡]MARS Bioimaging Ltd, Christchurch, New Zealand
[§]European Centre for Nuclear Research (CERN, Geneva, Switzerland)
[¶]HIT Lab NZ, University of Canterbury, New Zealand

***Abstract*—The MARS programme is developing spectral CT scanners to advance medicine. Our system is built upon the Medipix3RX ASIC developed by a CERN led collaboration. The Medipix3RX has 8 counters where some counters use charge summing technology to improve energy resolution. Our scanners include small bore scanners, pre-clinical systems used by our partners at the Mayo Clinic, Notre Dame University, and the University of Otago, and a large bore scanner (a human scale system in development). In this talk we demonstrate some of the applications, and publicly available datasets, that show how spectral CT can enhance pre-clinical and medical imaging. Our primary challenge for the future is to improve our reconstruction methods to generate artefact free, quantitative material volumetric datasets for clinical use.**

I. Introduction

The key scientific goal for the MARS programme is to develop scanners that enable the exploration of spectral CT images within medicine. In this paper, we present our current systems and their capabilities. We describe a range of applications in active research and provide some public datasets that demonstrate how spectral CT is useful in medical imaging. Lastly, we briefly describe our current reconstruction approach and discuss the challenges that we wish to solve in the near future.

MARS currently has two systems: a small bore scanner (used for current pre-clinical research), and a large bore scanner (a human scale system in active development). Both types share common design principles and common components to ensure that biomedical results may be readily translated between the two systems. Each system consists of three main parts: a scanner containing an energy resolving camera, an x-ray tube, a gantry to position the components, and a sample bed to position the subject; a data processing chain to reconstruct the spectral CT data and decompose the results into materials; and a visualisation and analysis tool. The gantry and sample bed differ in scale between the small and large bore scanners.

The small bore scanner is in active use around the world [1], [2]. The range of pre-clinical research that is ongoing with MARS system includes: multi-contrast imaging in mice, risk classification of atheromatous plaques, tumours in mice, quantifying the health of cartilage, scaffold implants to promote bone growth, quantification of fat and soft-tissues in meats, etc. These applications provide a wealth of MARS spectral CT datasets, some of which have been made publicly available including the raw, processed, and visualised data. It is our hope that these datasets, together with those related with this paper, can promote improvements in spectral CT reconstruction algorithms to produce artefact free, quantitative material volumetric datasets.

The reconstruction solution employed in the current MARS system adopts a two-step approach. First, the data is reconstructed into a series of attenuation volumes using common CT reconstruction methods. These attenuation volumes are then transformed via decomposition into a set of material volumes representing density in mg/ml. While this approach produces useful pre-clinical images, it leaves much to be desired. The material decomposition step, when performed after the reconstruction of attenuation volumes, has to contend with CT artefacts such as beam hardening, and noise. We believe that a one-step solution that reconstructs material volumes directly from the raw photon counts has the best potential to achieve high quality medical images.

Section II provides an overview of the MARS system. Section III introduces a range of current applications explored along with some datasets that are, or soon will be, publicly available. Section IV describes the general approach of our current reconstruction solution, and discusses the challenges that we face. Lastly, we conclude the paper with an overview of where we see spectral CT heading in the future.

II. MARS System

A MARS system is a complete solution consisting of the physical scanner, the image processing software, and the visualisation and analysis software. Each of these components are independent units. In this section, we describe the physical scanner along with an overview of the visualisation software.

A MARS scanner consists of an energy resolving camera, a standard x-ray tube, a gantry to position the camera and x-ray tube, a sample bed to position the subject, and software to control the operation and to interact with the user. There are two designs of MARS scanners; the small bore, and the large bore. The only difference between the two is the design of the gantry and the sample bed. This means that results may be readily translated between the two system designs.

DOI: 10.12059/Fully3D.2017-11-3111007

Fig. 1. A view of a MARS small bore scanner during assembly. The left shows the cabinet opened along with the internal lead-lined container. Center and right are two gantries in production revealing its structure, and the control circuitry.

A. Energy resolving, photon counting cameras

A MARS camera contains multiple CZT-Medipix3RX detector modules in linear arrays. These are photon counting detectors that can discriminate between x-ray energies. Cameras can range from 1 detector module to as many as are available.

Each Medipix3RX [3], [4] ASIC is bonded by Advacam [5] to 2 mm of Redlen CZT [6](the sensor material) such that the pixel pitch is 110 um. Together, they provide up to 8 energy bins of information. Typically, one bin provides the total photon count, four more operate in charge summing mode to improve the energy resolution, and the final three operate in single pixel mode.

For each detector, a single ARM based computer and FPGA performs the data readout. Within a single camera, each detector readout operates in parallel, providing simultaneous acquisitions across all detectors. Control and data transfer is achieved via standard Ethernet technologies.

B. The gantry and the sample bed

The small bore system can support samples up to 100 mm diameter and up to 270 mm length. It is embedded in a lead-lined stainless steel container inside a cabinet to provide a self-contained scanner that may safely operate anywhere. Fig. 1 shows the internal structure of the small bore gantry. The large bore gantry will be able to support samples up to 750 mm diameter, and up to 1200 mm length. As a human sized scanner, it is installed in a lead-shielded room.

A typical scan follows a helical path. To accomplish this, the gantry can rotate the camera and a 120kV x-ray tube around the sample bed. It uses a slip ring to provide continuous Gb Ethernet communication and power as it rotates. The camera can also be translated across the gantry to span subjects of greater diameter than its active length. For the small bore design, magnification can be altered via motors for both the camera and the x-ray tube. Alternatively, the magnification adjustments are manual for the large bore design. Collimators and x-ray filters are also motorized to restrict the x-ray beam to the imaged volume, and to provide a selection of aluminium and brass filters with a variety of thicknesses.

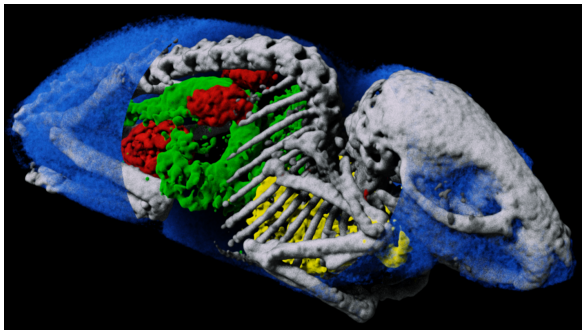

Fig. 2. MARS Vision 3D rendering: A mouse MD showing the separate channels of fat, water, gold (lungs), gadolinium (intestines), and iodine(kidney and bladder). Some material channels, such as water are transparent while others are opaque. A 3D magic lens further enhances the view of the central organs.

The sample bed is motorised to support continuous motion in and out of the scanner. In the small bore scanners, the sample bed can also move up and down, and left and right, to better position the subject.

The scan obtains sets of 2D energy-resolved projection images, $Q(p, c, \theta)$ where p labels the pixel, c labels the energy counter, and θ labels the helical angle. These are automatically pre-processed and stored in DICOM format [7]. This makes the raw data compatible for transfer to an institutional PACS. The 2D energy-resolved projection images are then ”reconstructed” into 3D energy-resolved volumetric datasets, $V(v, e)$ where v labels the voxel and e labels the energy bin. Finally the data is transformed into material volumetric datasets, $X(v, m)$ where v labels the voxel and m labels the material. All volumetric datasets $V(v, e)$, and $X(v, m)$ are stored using DICOM.

C. MARS Vision

To visualise the MARS spectral CT data, a comprehensive viewing and analysis tool has been developed called MARS Vision. Visualisation techniques include standardised diagnostic 2D slice views, 3D volume rendering, 3D mesh visualisation, and minimum and maximum intensity projection.

For both 2D and 3D rendering options, attenuation and material channels can be fused into hybrid images. Typically, attenuation channels provide context, while material channels provide specific, quantitative information. A “Magic Lens” tool allows sections to be displayed using a different set of fused channels. Fig. 2 illustrates a MARS Vision 3D rendering of a multi-contrast mouse showing a series of materials along with a “Magic Lens” to highlight the central organs.

Measurement and analysis tools are supported as part of the visualisation package. Both 2D and 3D regions of interest can be created from primitive shapes (lines, angles, ellipses, and polygons) and then analysed. This allows the basic radiology workflow to function within MARS Vision.

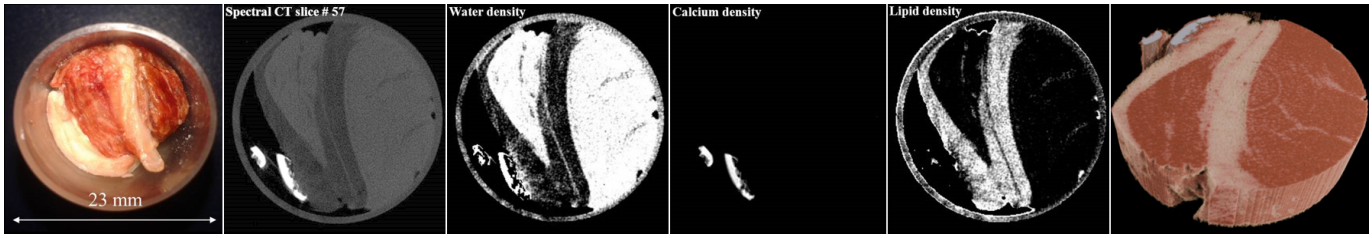

Fig. 3. The results from a scan of a cut of lamb meat. From the left is a photo of the sample, a slice from the attenuation volume, the water channel, the calcium channel, the fat channel, and a volume rendering of the materials using a natural colour scheme.

MARS Vision also includes support for zSpace™ [8], [9], a 3D stereoscopic monitor that fuses head tracking, along with a 3D stylus for a unique interactive experience. Stereoscopic images are synchronised with the regular 2D slice views to allow for an enhanced radiology workflow. Here, 3D manipulation is achieved via the zSpace stylus to find appropriate 2D transverse planes, and analysis is then performed on these 2D planes with the standard mouse. This hybrid approach has been tested with medical students and radiologists (residents) and was found to be easy to learn and easy to use. It has been shown to improve the accuracy of diagnosis [10].

III. Applications of MARS Imaging

The MARS small bore system has already been used in a wide range of pre-clinical research applications [11]. In this section, we demonstrate a few of these applications. In some cases, we have released complete datasets to the public domain including raw and preprocessed projections, and energy and material volumes.

A. Quantifying fat, muscle, and bone in meats

A large number of clinical issues and commercial industries are interested in separating fat, muscle, and bone. As a preliminary study of this problem, a slice of lamb was scanned, and decomposed into fat, water (muscle), and calcium (bone).

Fig. 3 shows the results of the scan alongside a photo of the sample. This image also illustrates the data output from the MARS system. The attenuation volume slice shown reveals all materials together as a standard CT image would. The material volume slices show the output from the material decomposition. Lastly, the 3D rendering shows the material volumes together as a natural representation of the sample. This dataset was published by Aamir et. al. in the Journal of Instrumentation [12] and made public on http://hdl.handle.net/10092/8531.

B. Health in cartilage and bone

A study of cartilage health aims to use spectral CT to quantify the amount of glycosaminoglycans (GAG) [13]. The current hypothesis is that the GAG content directly relates to the health of the cartilage. It is also known that iodine tends to diffuse to areas of low GAG content. Therefore, when an iodine based contrast agent is used, the presence of iodine indicates the lack of presence of GAG.

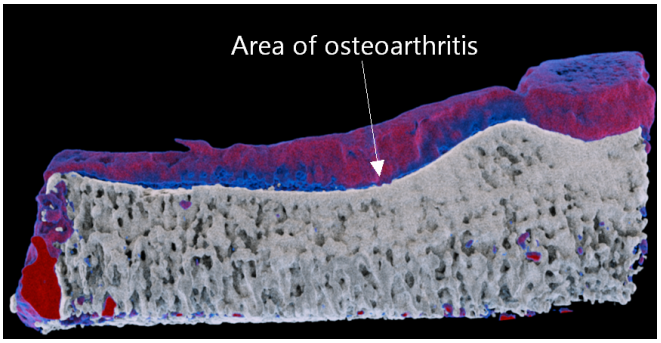

Fig. 4. A rendering showing the presence of iodine in a cartilage/bone sample from a tibial plateau. Iodine is coloured as a gradient from blue (less) to red (more). Bone is shown in greyscale. The red shades indicate the presence of osteoarthritis (shown) in the middle of the sample.

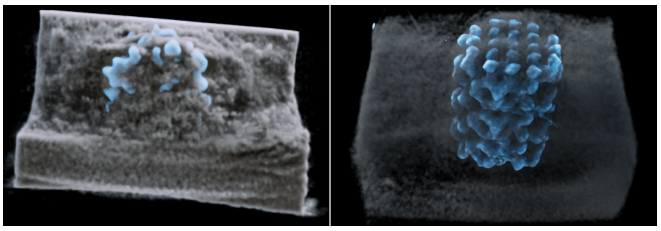

Fig. 5. A rendering showing the interface between bone and a metal scaffold. The left image focus is on the bone, while the right image focus is on the scaffold. Both cases show a clear distinction between the two.

An initial study of quantifying GAG took a human excised cartilage sample from the tibial plateau, saturated the sample with Hexabrix (iodine), and then scanned the sample. The material decomposition split the data into fat, water, iodine, and calcium (bone). Fig. 4 shows the result when viewing the iodine and calcium channels from the dataset. The image uses a colour gradient (blue to red) to show where iodine has the most presence. The image demonstrates that the MARS system can be used to inversely map GAG content in cartilage.

Bone ingrowth to scaffolds is an important area of research as many modern orthopedic implants are fixed in place by bone growing through a porous surface. Studying the bone-scaffold interface is important in designing new implants. Key information is good imaging at the bone/metal interface and quantification of calcification of the bone as it grows. Fig. 5 illustrates the results from an implant of a scaffold into a section of bone that demonstrates that the bone/metal interface

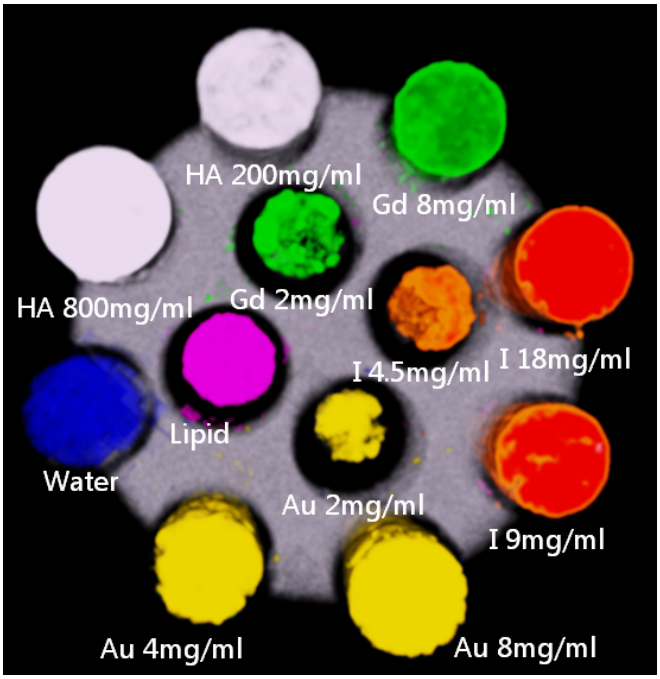

Fig. 6. A rendering of a spectral phantom (right) containing concentrations of gold (yellow), gadolinium (green), iodine (red), calcium (white) alongside water (blue) and lipid (purple). This image demonstrates that high Z materials can be identified down to at least 2 mg/ml.

is clearly revealed.

C. Separation of High-Z materials

Various studies are ongoing that aim to separate multiple contrast agents in a single scan. In this example, concentrations of four high Z materials alongside water and lipid positioned in a 12 hole phantom and scanned. The high Z material concentrations include gold (2, 4, and 8 mg/ml), gadolinium (2, and 8 mg/ml), iodine (4.5, 9, and 18 mg/ml), and calcium (200 and 800 mg/ml) in hydroxyapatite. Fig. 6 demonstrates the outcomes of the study. As can be seen all of the materials have been correctly identified with some minor issues at the lowest concentrations of gold, gadolinium and iodine. Such studies are also often used to calibrate the system for biological scans, such as the multi-contrast mouse shown in Fig. 2.

A similar study was published together with data by Moghiseh et al [14]. In this case, the study investigates the quality of the material separation and shows how well each concentration is identified and misclassified.

IV. Spectral CT reconstruction and material decomposition

Spectral CT reconstruction presents a new set of opportunities and challenges for medical imaging. In this section, we outline our current approach and discuss its shortcomings and strengths.

A. MARS image processing chain

The current image processing is achieved through a chain consisting of five algorithms over two programs. The first program is the reconstruction software that takes raw data (in the form of scan data, flat-field data, and a mask) and converts it to a set of attenuation volumes as functions of energy. This includes four algorithms for flat-field correction, inpainting, ring filtration, and spectral CT reconstruction. The second program is a dedicated piece of software for the material decomposition algorithm that converts the attenuation volumes to a set of material volumes.

The raw data represents photon counts from the 8 counters in the Medipix detector. Each counter's energy range extends from a set low threshold to a common kVp set for the x-ray tube. This means that the raw data represents a set of overlapping broad energy bins.

The mask is a map that indicates the reliability of each pixel from each detector in the camera. It is derived from pixel measurements made prior to the scan. Using the mask, faulty pixels may be removed.

The flat-field data represents open beam counts for the same selection of energy bins, and the same selection of camera positions over the scan. Flat-field correction uses a standard algorithm of dividing the raw data by the corresponding flat-field data to correct for inter-pixel variation and variation over the x-ray beam. A global mean flat-field count per energy bin then returns the corrected raw data back to counts.

The inpainting algorithm uses a series of small median filters to fill in small regions of dead pixels. Its only mandate is to slightly improve the condition of the data before ring filtration. Large dead regions remain untouched.

The ring filtration algorithm uses two directional median filters. The first median filter covers a local "cross-shaped" region in the projection images to detect the difference between a pixel and its neighbours (the potential error of the pixel). The second median filter is a 1D filter between projection images (or along the angle axis of the sinogram) to find the static error of the pixel. This static error is then subtracted from the data to yield a cleaner result.

The reconstruction algorithm uses an iterative, one-step approach to reconstruct a set of adjacent, non-overlapping attenuation volumes from the raw overlapping broad energy bins. The raw data is not subtracted in any way before or during reconstruction. This approach means that the raw energy bins influence multiple attenuation volumes, and this has an averaging effect on the noise. In essence, it exploits the fact that although the energy signal is unique to each energy bin, the geometric signal (where boundaries are located) is identical for all energy bins. The iterative algorithm used is based on ordered subsets expectation maximisation [15].

The reconstruction algorithm also adopts a multi-stage approach where it initially reconstructs voxels that are 8 times larger than requested. Later on this is repeatedly subdivided, for a total of four stages, until the requested voxel size is reached. This approach allows for the reconstruction to proceed quickly. It is also is a weak form of a sparsity constraint as a large voxel is the same as a set of small voxels with the same value. Lastly, the larger the voxel, the more pixels from the projection images will contribute to

it. This means that the presence of dead regions will have less of an effect. This is particularly useful during the initial reconstruction stages where the effects of dead regions are the most significant.

The material decomposition algorithm adopts a combinatorial approach. It defines a set of acceptable material relationships (such as permitting water and iodine in the same voxel but not iodine and gold) and best fits the data to it. The calibration for these relationships is derived from scans of known phantoms.

B. Challenges

In section III, we demonstrated some applications that show how the our current results already benefit pre-clinical research by providing novel information in medical imaging. However, it is clear that much more can be done.

The approach to material imaging that we have taken can be described as a post-reconstruction solution. This means that the data is converted to attenuation volumes and then decomposed to material volumes. This has a few drawbacks.

Firstly, any noise and blurring in the attenuation volumes will hinder the material decomposition result. This is particularly an issue with blurring where the outlines of objects can be misclassified. In order to reduce the affects of noise, denoising algorithms can be used. However, this simply increases the issues of misclassification at object boundaries.

However, the biggest issue is the artefacts due to beam hardening (streaks and cupping). The use of narrow adjacent, non-overlapping energies reduces the impact of beam hardening, but the effects are still strong for dense materials. It would be possible to invest in a beam hardening correction algorithm. However, as beam hardening is actually the novel part of the spectral CT signal, any reduction of that signal brought about through a monochromatic approximation would be an inferior solution.

An alternative approach considered by many others (see, for example [16], [17]), is some form of pre-reconstruction material decomposition. This would split the projection data into materials and then reconstruct the material projections into material volumes. This has the advantage that polychromatic methods could be employed to eliminate beam hardening completely.

Pre-reconstruction approaches suffer from two major drawbacks. Firstly, they usually operate on a per-pixel basis in the projection space (or a local region). This means that the full effect of the noise in the pixel would have to be dealt with. In comparison, a voxel is the accumulated result from a large number of rays. Therefore, the number of photons contributing to a voxel value is significantly higher, and the noise, significantly less.

The second major drawback is the lack of sparsity constraints. The number of materials in a voxel is generally limited. However, the number of materials in a ray is not. Therefore, pre-reconstruction methods can not directly exploit the available material sparsity to better focus on more accurate solutions.

The final option is a one-step approach to directly convert from the raw photon counts to material volumes. This approach would allow the best of both worlds as sparsity constraints can be fully employed, and polychromatic algorithms could be developed. Naturally, there is a drawback in that such an approach is complex. It is challenging to find a solution that both works, and is efficient enough to operate in a commercial research or clinical setting.

V. Conclusion

The MARS team has developed a complete suite of tools for research into spectral x-ray imaging. These tools include the scanner (small bore and large bore designs), CT reconstruction and material decomposition algorithms, and visualisation and analysis software. The system is already capable of supporting pre-clinical research and has done so for a variety of studies around the world. In the case of the lamb meat study, the data was made public some years age to support further research into spectral CT reconstruction algorithms and visualisation techniques. We provide further more recent datasets with the publication of Rajendran et. al's article in the Journal of Instrumentation [18]. The four datasets from this paper are available at http://hdl.handle.net/10092/8851.

The reconstruction and material decomposition algorithms currently used are effective for some pre-clinical applications. It achieves this via a post-reconstruction material decomposition solution. In a one-step process, the reconstruction simultaneously generates a set of adjacent, non-overlapping attenuation volumes (as functions of energy bins) directly from the set of projection images using the raw overlapping energy bins of a Medipix3RX ASIC. The material decomposition then converts the set of attenuation volumes to material volumes. However, it is clear that much more could achieved if better algorithms were to be discovered and used. Currently, we feel that a one-step algorithm from raw data directly to material volumes would have the most potential in producing artefact free, quantitative images.

Throughout this paper, we have shown the final output of our system to be quantitative material volumes represented in mg/ml. We strongly feel that material volumes are the future for CT datasets as they are both highly specific, and directly relate to simple physical measurements. In addition, as the relationship between attenuation and density is linear, attenuation volumes for monochromatic energies can always be derived from material volumes. So traditional clinical methods can always be used, and more importantly, new methods can be established. Therefore, we feel that the challenge of generating accurate, clean material volume images is the primary challenge for CT today.

Acknowledgment

The authors would like to thank the MARS team that participated towards this work in all its various aspects. We also acknowledge financial support from the New Zealand Ministry of Business, Innovation and Employment (MBIE)

grant UOCX1404. Finally, we thank the Medipix 3 collaboration that drove the Medipix detector technology forward making spectral CT imaging possible.

REFERENCES

[1] S. M. Jorgensen, A. J. Vercnocke, D. S. Rundle, P. H. Butler, C. H. McCollough, and E. L. Ritman, "Evaluation of a photon counting Medipix3RX CZT spectral x-ray detector," *Proc SPIE Int Soc Opt Eng*, Oct 2016.

[2] N. Welding. (2015) The transformation of cancer imaging: From shades of gray to living color. Website. University of Notre Dame. [Online]. Available: http://news.nd.edu/news/the-transformation-of-cancer-imaging-from-shades-of-gray-to-living-color/

[3] Medipix. Welcome to the medipix homepage! Website. CERN. [Online]. Available: https://medipix.web.cern.ch/medipix/index.php

[4] R. K. Panta, M. F. Walsh, S. T. Bell, N. G. Anderson, A. P. Butler, and P. H. Butler, "Energy calibration of the pixels of spectral x-ray detectors," *IEEE Transactions on Medical Imaging*, vol. 34, no. 3, pp. 697–706, March 2015.

[5] Advacam. (2017) Advacam imaging the unseen. Website. Advacam. Advacam Oy, Tietotie 3, 02150 Espoo, Finland. [Online]. Available: http://advacam.com/en/

[6] REDLEN. (2017) About redlen. Website. Redlen Technologies. Redlen Technologies, 123 1763 Sean Heights, Saanichton, BC, V8M 0A5. [Online]. Available: http://redlen.ca/

[7] *DICOM Part 3: Information Object Definitions*, National Electrical Manufacturers Association Std., 2014b. [Online]. Available: http://medical.nema.org/medical/dicom/current/output/html/part03.html

[8] zSpace. (2017) The ultimate learning experience. Website. zSpace, Inc. 490 De Guigne Drive, Ste 200, Sunnyvale, CA 94085. [Online]. Available: https://zspace.com/

[9] R. Aras, Y. Shen, and A. Noor, "Quantitative assessment of the effectiveness of using display techniques with a haptic device for manipulating 3d objects in virtual environments," *Advances in Engineering Software*, vol. 76, pp. 43 – 47, 2014. [Online]. Available: http://www.sciencedirect.com/science/article/pii/S0965997814000933

[10] V. B. H. Mandalika, A. Chernoglazov, M. Billinghurst, C. Bartneck, M. Hurrell, N. de Ruiter, A. Butler, and P. Butler, "A hybrid user interface improving radiological diagnosis," *In Preparation*, 2017.

[11] R. Zainon, J. P. Ronaldson, T. Janmale, N. J. Scott, T. M. Buckenham, A. P. H. Butler, P. H. Butler, R. M. Doesburg, S. P. Gieseg, J. A. Roake, and N. G. Anderson, "Spectral ct of carotid atherosclerotic plaque: comparison with histology," *European Radiology*, vol. 22, no. 12, pp. 2581–2588, 2012. [Online]. Available: http://dx.doi.org/10.1007/s00330-012-2538-7

[12] R. Aamir, A. Chernoglazov, C. J. Bateman, A. P. H. Butler, P. H. Butler, N. G. Anderson, S. T. Bell, R. K. Panta, J. L. Healy, J. L. Mohr, K. Rajendran, M. F. Walsh, N. J. A. de Ruiter, S. P. Gieseg, T. Woodfield, P. F. Renaud, L. Brooke, S. Abdul-Majid, M. Clyne, R. Glendenning, P. J. Bones, M. Billinghurst, C. Bartneck, H. Mandalika, R. Grasset, N. Schleich, N. Scott, S. J. Nik, A. Opie, T. Janmale, D. N. Tang, D. Kim, R. M. Doesburg, R. Zainon, J. P. Ronaldson, N. J. Cook, D. J. Smithies, and K. Hodge, "MARS spectral molecular imaging of lamb tissue: data collection and image analysis," *Journal of Instrumentation*, vol. 9, no. 02, p. P02005, 2014. [Online]. Available: http://stacks.iop.org/1748-0221/9/i=02/a=P02005

[13] K. Rajendran, C. Lobker, B. S. Schon, C. J. Bateman, R. A. Younis, N. J. A. de Ruiter, A. I. Chernoglazov, M. Ramyar, G. J. Hooper, A. P. H. Butler, T. B. F. Woodfield, and N. G. Anderson, "Quantitative imaging of excised osteoarthritic cartilage using spectral CT," *European Radiology*, vol. 27, no. 1, pp. 384–392, Jan 2017.

[14] M. Moghiseh, R. Aamir, R. K. Panta, N. J. A. de Ruiter, A. I. Chernoglazov, J. L. Healy, A. P. H. Butler, and N. G. Anderson, "Discrimination of multiple high-Z materials by multi-energy spectral CT a phantom study," *JSM Biomed Imaging Data Pap*, vol. 3, no. 1, p. 1007, 2016.

[15] H. M. Hudson and R. S. Larkin, "Accelerated image reconstruction using ordered subsets of projection data," *IEEE Transactions on Medical Imaging*, vol. 13, no. 4, pp. 601–609, Dec 1994.

[16] C. O. Schirra, E. Roessl, T. Koehler, B. Brendel, A. Thran, and R. Proksa, "Maximum likelihood CT reconstruction from material-decomposed sinograms using fisher information," in *2011 IEEE Nuclear Science Symposium Conference Record*, Oct 2011, pp. 4063–4065.

[17] R. A. Nasirudin, R. Tachibana, J. J. Nppi, K. Mei, F. K. Kopp, E. J. Rummeny, H. Yoshida, and P. B. Nol, "A comparison of material decomposition techniques for dual-energy CT colonography," *Proc SPIE Int Soc Opt Eng*, 2015.

[18] K. Rajendran, M. F. Walsh, N. J. A. de Ruiter, A. I. Chernoglazov, R. K. Panta, A. P. H. Butler, P. H. Butler, S. T. Bell, N. G. Anderson, T. B. F. Woodfield, S. J. Tredinnick, J. L. Healy, C. J. Bateman, R. Aamir, R. M. N. Doesburg, P. F. Renaud, S. P. Gieseg, D. J. Smithies, J. L. Mohr, V. B. H. Mandalika, A. M. T. Opie, N. J. Cook, J. P. Ronaldson, S. J. Nik, A. Atharifard, M. Clyne, P. J. Bones, C. Bartneck, R. Grasset, N. Schleich, and M. Billinghurst, "Reducing beam hardening effects and metal artefacts in spectral CT using Medipix3RX," *Journal of Instrumentation*, vol. 9, no. 03, p. P03015, 2014. [Online]. Available: http://stacks.iop.org/1748-0221/9/i=03/a=P03015